

Design of a Breathing, Anthropomorphic Phantom for Positron Emission Tomography

David G. Black, *Student Member, IEEE*, Yas Oloumi Yazdi, Jeremy Wong, and Dr. Ivan Klyuzhin

Abstract— Patient motion during Positron Emission Tomography (PET) scans can be a major detriment to image quality, leading to quantification errors and radiologists potentially missing malignant lesions. The primary source of movement in thoracic PET scans is respiratory, followed by cardiac motion. These problematic effects can be mitigated to a degree using motion correction algorithms. In order to further develop, improve, and test such algorithms, anthropomorphic phantoms with accurate anatomy and realistic motion are needed. In this work we present such a phantom, which builds off the state of the art in humanoid phantom anatomy by adding elastic lungs with a highly controllable, realistic breathing mechanism to an existing, proven anatomically accurate phantom. The breathing mechanism can produce a plethora of custom respiratory wave-forms with breathing rates up to 25 breaths per minute and tidal volumes up to 1200mL. It does not decrease the anatomical accuracy in any way through the addition of mechanisms or actuators inside the torso. The full mechanical design is described in this paper, as well as a software application with graphical user interface which was developed to plan and visualize respiratory patterns. Finally, tests were carried out to validate the effectiveness and accuracy of the mechanism. With flexibility in the desired respiratory pattern, as well as the potential to add cardiac motion, this phantom will facilitate future work in developing new motion correction algorithms and evaluating the effect of motion on image quantification.

Index Terms— Biomechanical modeling, Lung, Motion compensation and analysis, Nuclear imaging

I. INTRODUCTION

POSITRON Emission Tomography (PET) is a nuclear medicine imaging modality which captures tissue function rather than anatomy. It is heavily used in brain disease and oncological diagnosis, as well as treatment planning, and research. The patient is given a low dose of a radioligand, or biologically active molecule tagged with a radioisotope which undergoes β^+ decay. A commonly used radioligand in oncology is ^{18}F -FDG (fluorine-18-tagged fluorodeoxyglucose), which acts as a glucose analog, gathering at sites of malignant and proliferating tumor cells due to their predominantly non-oxidative glycolysis. Here, the emitted positrons annihilate with electrons in the surrounding tissue, releasing pairs of 511keV photons with opposite momenta. These photons are

David G. Black, Yas Oloumi Yazdi and Jeremy Wong are with the Department of Physics and Astronomy, University of British Columbia, Vancouver, Canada (e-mail: dgblack@ece.ubc.ca).

Dr. Ivan Klyuzhin is with the BC Cancer Research Centre, Vancouver, Canada (ivan.skn@outlook.com)

measured at opposite sides of the cylindrical PET scanner, and 3-dimensional images are reconstructed over millions of such coincidence events. The spatial resolution of full-body, clinical PET scanners is limited to around 5mm [11], yet respiratory and cardiac motion can greatly degrade the image quality, leading to resolutions closer to 10mm in practice [25]. Since PET scans take on the order of 5 – 60 minutes [11], breath-holding is infeasible, and any movement in the subject being measured leads to blurring of the image. In the majority of patient scans, the predominant motion is respiratory and can lead radiologists to miss malignant lesions, or cause Standardized Uptake Value (SUV) and lesion volume quantification bias. Hence, a large amount of research is being performed on how to correct for such motion.

Current motion correction focuses on respiratory gating, in which image acquisition is split into temporal bins, separated by 'gates', which always coincide with the same portion of the respiratory cycle [14]. Each bin produces its own image, with photons always captured while the tissue is in about the same location. Hence, motion during each bin is minimized, though photon count in every separate image is also reduced, leading to noisier images [4]. The images are transformed and subsequently recombined to improve the counting statistics. Gating occurs either through hardware or software triggering, the latter of which has been shown to be favorable [2]. An alternative approach is through Data-Driven Motion Correction algorithms [1].

While more sophisticated motion correction algorithms exist and have been shown to improve image quality [19] [26] [35], the development and testing of new algorithms is very difficult given the tight patient regulations, the cost of scanner time, and the lack of a 'ground truth' in patient studies. Consequently, there is little literature which shows definitively that motion correction provides a clinical advantage in tumor identification. Without a large body of supporting evidence, the resultant additional training and equipment requirements, as well as increased scan time lead most radiologists to opt not to use the available motion correction algorithms on their PET scanners [2]. However, it is known that quantitative analysis and image quality are impacted by motion correction [19] [26] [35], so it remains to be shown, for example through direct comparison to a known ground truth, that this translates to a clinical advantage. Such analysis could impact the quality of care of the millions of patients who are scanned each year [13].

Thus, it is essential to develop an efficient method of testing

Name	PET/CT/MRI Compatible	Cardiac Motion	Respiratory Motion	Liver Motion	Skeletal Structure	Lesions
This work	✓/✓/×	✗	✓	✓	✓	✓
DANN [6] [7]	✓/✓/×	✗	✗	✗	✓	✓
Wilhelm [17]	✓/✓/✓	✓	✓	✓	✗	✓
Alderson [12]	✓/✓/×	✓	✓	✗	✓	✗

TABLE I
COMPARISON OF EXISTING ANTHROPOMORPHIC PHANTOMS OF INTEREST.

motion correction algorithms and characterising the effect of the motion on quantitative data derived from PET images. For many other developments in PET, including characterizing the impacts of time-of flight [6] and various 3D reconstruction techniques [7], phantoms were used. These are devices designed to have similar X-ray and gamma ray attenuation properties as human tissue and are used to test and calibrate scanners. PET phantoms usually consist of a clear plastic shell containing a radioactive water solution and any number of different plastic shapes that can be used to calibrate scanners, find their resolution limits, or simulate a human body. In order to characterise the effect of motion on image quantification, an anthropomorphic phantom is needed with the ability to move and breathe like a human. This work sets out to address that need.

A. Existing Anthropomorphic Phantoms

Dr. Dan Kadomas et al. developed a Designated ANthropomorphic phaNtom (DANN), which contributed significantly to PET being routinely used in clinics [6] [7]. As far as we know, its anatomic accuracy is unmatched at time of writing. The phantom consists of a human torso with rib-cage, spine, lungs, heart, and liver, as well as a brain phantom, and a pelvic phantom with bladder, all of which have realistic 511keV attenuation coefficients. Radioactive lesions can be placed anywhere in the torso. While highly realistic in PET and CT scans, this phantom is completely static and thus provides no direct value for studies dealing with motion effects. The phantom described in this paper uses the torso shell and ribcage of DANN, but adds elastic lungs with trachea, and a driving mechanism to create realistic respiratory motion.

Other phantoms have been developed in the past, each of which solves a subset of the problems associated with respiratory motion modeling. These phantoms are compared

in Table I and below. Numerous others also exist that are not mentioned in Table I because they have only cardiac motion [16] [30] [5].

While Wilhelm [17] has the most realistic overall motion of any existing device, it lacks any bone structure, which greatly affects the realism of the phantom as bone attenuation plays an important role. Conversely, Alderson [12] has bones as well as respiratory and cardiac motion, but its anatomy is simplified and not particularly accurate. It also does not support the addition of lesions, which are key in any studies investigating the effect of motion on quantification and motion compensation strategies.

B. Aim and Scope

The goal of this work was to create an anatomically accurate phantom with realistic respiratory motion modeling for studies on the effect of motion on PET image quantification. This phantom aims to achieve the following:

Anatomical Accuracy

- Builds off the static anatomical accuracy of DANN and achieves realistic lung motion.
- Avoids any unrealistic parts like connecting rods, metal components, etc. in the torso.
- All materials carefully selected with reference to mass attenuation coefficients [24] to resemble human tissue under gamma and x-rays.

Breathing Control

- Able to achieve a wide range of typical breathing rates and tidal volumes. Namely, at least up to 25 breaths per minute at 1L tidal volume. (Typical relaxed breathing is 500mL tidal volume at 15-20 breaths per minute [34].)
- Has highly controllable, repeatable, consistent breathing motion to generate high quality data, but also has the ability to include occasional disrupted breaths or inconsistencies, as would happen in a real patient.

In addition, safety is a concern, as the phantom will be filled with 17.3L of radioactive solution (300 to 1000MBq of radioactivity per scan). The design must avoid any leaks, and completely eliminate the possibility of sudden large spills. Easy fill-ability of the phantom is also desirable to avoid radiation exposure.

While the focus in this work was respiratory motion, the expansion and compression of the lungs will indirectly push the liver and other organs, as it does in humans. The phantom also has the potential to add cardiac motion in future.



Fig. 1. DANN phantom, upon which this work builds

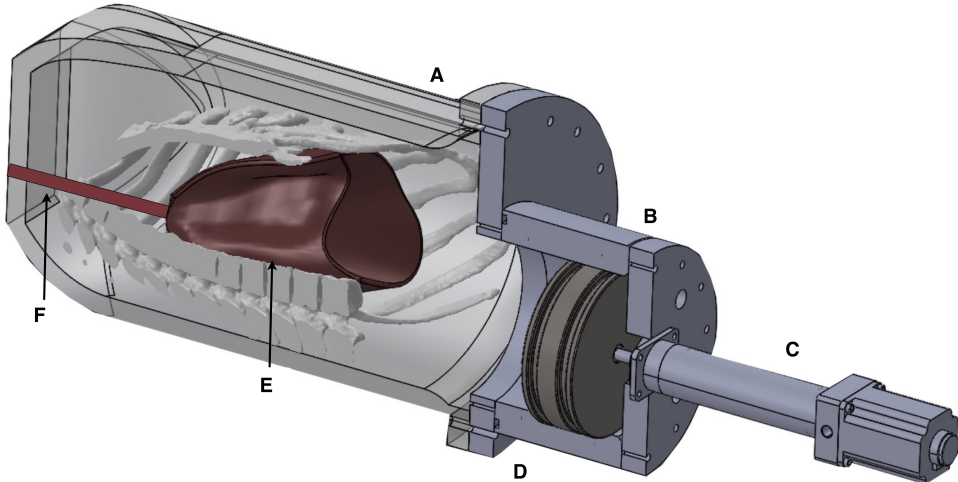


Fig. 2. Overview of phantom design. A: existing thorax shell and bone structure (liver and heart included but not pictured) (Section I-A). B: Piston and cylinder for volume modulation. C: linear actuator (Section IV). D: custom-designed base-plate allows compatibility with existing DANN phantom. E: flexible lung inserts of Chlorosil-35 silicone elastomer. F: breathing tubes (trachea) connect lungs to atmosphere to allow breathing (Section III).

II. DESIGN OVERVIEW

The addition of lung motion to the DANN phantom involves three main components: elastic lungs, an actuation method, and control electronics. The overall structure can be seen in Fig. 2. The lungs are located inside the rib cage of the existing DANN Phantom. They are connected to the atmosphere by breathing tubes (trachea), which can be sealed. The actuating mechanism is placed below the phantom, where the pelvis of a human would be. It is outside the field of view of the PET scanner so as not to create image artefacts. The phantom operates by piston-actuated passive breathing, as explained below and seen in Fig. 3.

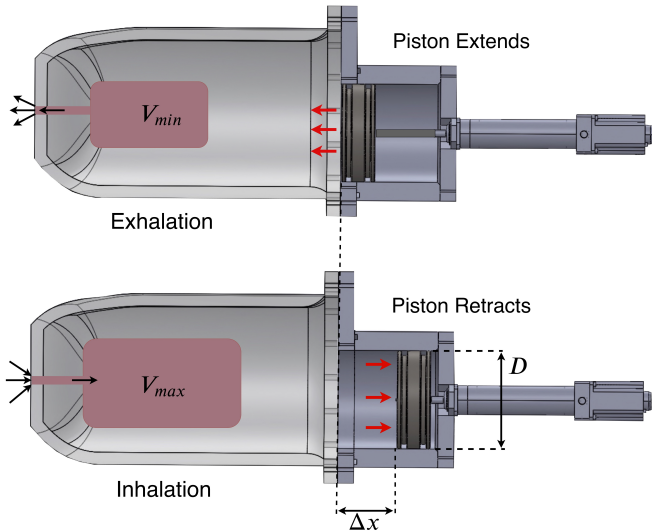


Fig. 3. Respiration modeling by modulating the volume of the phantom, mediated by incompressible fluid. Air flows into and out of the lungs through the trachea as the piston extends and retracts.

Achieving respiratory motion with the lungs is possible through a variety of mechanisms, which fall into two main

classes. First, the lungs can be directly inflated using air pumps or compressors. This is the most obvious approach, but involves a number of complicating factors. The lung volume cannot simply increase inside a sealed, rigid torso filled with incompressible water. An overflow tube or expanding section of the torso would be required. The former would create the risk of leakage, while the latter would require a powerful compressor. Furthermore, control is much more difficult with a pneumatic system and would require a great increase in complexity.

The second, and preferred method is to instead modulate the volume or pressure of the whole phantom. Since the phantom is sealed, rigid, and entirely filled with incompressible water, except for the air-filled lungs, changing its volume by ΔV induces an equal volume change of ΔV in the lungs. Instead of compressing the air in a sealed set of lungs, the pressure requirement of the actuating mechanism can be dramatically decreased by opening the lungs to the atmosphere once the phantom has been filled and sealed. Contrary to intuition, the lungs will not collapse under the pressure of the water since the water volume is constant, and cannot expand to fill the vacant space created if the lungs were to collapse. In effect we have created a relative negative pressure in the liquid above the lungs, just as human breathing relies on negative intrapleural pressure. Now, when the volume of the torso is changed, that volume of air is simply expelled to or sucked in from the atmosphere (See Fig. 3).

In DANN, all the organs and ribs are held in place by highly porous, compressible, open-cell foam. This serves the dual purpose of allowing lesions to be placed arbitrarily in the torso, and of adding tissue-like inhomogeneity to the image. There are two possible ways in which the moving lungs can be placed in the foam: (1) the foam is cut out to the size of the lungs in their most contracted form and the expansion of the lungs is able to apply enough force to compress the foam, or (2) the foam is cut to the size of the lungs in their maximum expanded state, leaving an empty space around the lungs when

they are contracted. The former is preferable but more difficult to achieve, and testing remains to be done to determine which method is more feasible. Even without the foam, the lungs are held in place by the breathing tubes and prevented from floating up by the ribs.

To prepare the phantom for imaging, the following steps are taken:

- 1) The lungs, organs, and bones are positioned inside the thorax.
- 2) The lungs are inflated to their maximum capacity and sealed.
- 3) The base plate is attached, and the piston is moved to its most retracted position (i.e. the phantom is at maximum volume).
- 4) The torso is turned upright (without the linear actuator taking any load), and completely filled with radioactive water solution using the ports in the neck.
- 5) The torso is sealed, and the lungs opened to the atmosphere.

Since the torso is rigid and sealed, its volume cannot change, so the lungs remain inflated. At this point, the lung volume can be fine-tuned by opening the water-filling port while pumping air into the lungs through the breathing tube valve using a manual pump, or releasing air through the same valve. Thus, any small changes or issues can be rectified.

With the phantom set up, the user can define a wide variety of respiratory patterns, rates, and volumes using the software described in Section V. The piston then moves along the defined trajectory for the duration of a scan, causing the lungs to expand and contract due to the change in pressure (See Section IV). The piston motion can also be coupled directly to the lungs using thin cables, which are not visible in the PET scan. The next three sections explain the lungs, breathing mechanism, and software in more detail.

III. LUNGS

The lungs were derived from a CT scan of an adult, male lung and simplified using mesh editing software to reduce the cardiac notch and make the right and left lungs symmetrical (Figure 4). This was done primarily for ease of fabrication, but also to avoid unpredictable expansion and contraction of complex shapes. The lungs are manufactured from Chlorosil-35 (Ottobock, Germany), a two-part, silicone-based elastomer with Shore A hardness 35. Following high temperature vulcanization, this material is durable, long-lasting, and thermostable, yet flexible to allow inhalation and exhalation. The material was tested and recommended by Schäfers et al. [17]. It resembles soft tissue under gamma radiation, as will be confirmed through testing conducted in a PET scanner in Section VI.

The lungs are designed to be a realistic adult size after normal exhalation, with a volume of 1650ml each. This ensures that during normal breathing the lungs only expand, and do not compress or fold in an unpredictable manner. The dimensions of the CAD model are approximately 18.00cm (height) by 10.26cm (width) by 12.75cm (depth). The lungs have uniform wall thickness and can be coupled to the piston using thin cables in order to achieve the desired flex pattern.

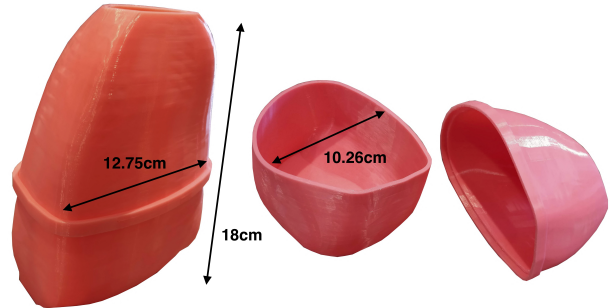


Fig. 4. Two-part, 3d-printed negative mold of the lungs used to create a dental plaster positive onto which the silicone elastomer is rolled. The lack of a seam inside the mold ensures a smooth plaster positive.

This causes the ratio of axial to lateral expansion of the lungs to be anatomically realistic [20], as is described more in Section IV. Alternatively, the Chlorosil can be strategically rolled on thicker in parts so the lungs flex more realistically; ie. thicker portions expand less. This has yet to be tested.

In addition, an air-tight, 3D-printed adapter (Fig. 5) will be attached medially near the top points of both lungs to connect air tubes which lead to the outside of the phantom, much like bronchi connecting to the trachea. One of three sealable ports in the neck area of the phantom provides the inlet for the breathing tubes. The lungs will be held in place in the superior/inferior axis using these air tubes, and in the lateral and anterior/posterior axes using the rib cage. At the inlet of the tubes, at the neck of the phantom, a sealable valve will make it possible to pressurize the lungs. The lungs also have pockets for radioactive lesion inserts.

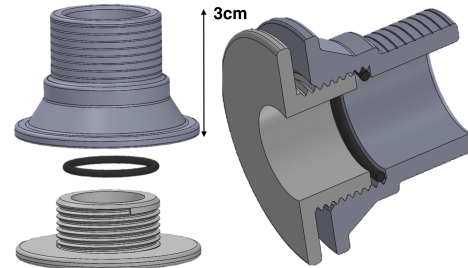


Fig. 5. Thru-hull fitting used to attach trachea to the lungs. The lung silicone is compressed between the twin flanges and, along with the O-ring, creates a water and air-tight seal.

A. Lung Manufacture

The manufacturing process is outlined below.

- 1) Negative mold is 3D-printed in two halves out of poly-lactic acid (PLA). This is due to size constraints in 3D-printing.
- 2) Dental plaster is then poured into the negative mold using the hole at the base.
- 3) Once the plaster has dried, it is extracted from the mold and put in a polyvinyl alcohol (PVA) bag. This bag prevents the Chlorosil catalyst from reacting with the plaster.
- 4) The Chlorosil is then rolled onto the positive dental plaster mold of the lungs.

- 5) Small pockets of silicone are placed on the lungs to provide locations for lesion insertion.
- 6) The dental plaster with the rolled Chlorosil is placed in an oven at 200°C for 12 hrs to cure the Chlorosil.
- 7) A thin piece of stiffer plastic with a mounting point for a cable is placed in a silicone pocket at the base of each lung. In this way a thin cable can optionally be used to couple the lung motion to the piston for optimal realism.
- 8) The mold is removed from inside the Chlorosil-35 lungs through the breathing hole to which the trachea will be attached. This is possible because the material is highly flexible.

IV. BREATHING MECHANISM

To modulate the volume, both a rubber diaphragm membrane across the phantom base and a piston mechanism were considered. We first constructed a to-scale diaphragm using $\frac{1}{8}$ " thick, 30A Shore durometer neoprene rubber and performed some simple tests of water proofing, load requirement, and resilience. By stacking known weights onto the diaphragm and measuring the deflection, we determined how much force was required to move the membrane by a certain amount. The results are plotted in Fig. 6. To achieve the desired lung volume change, the diaphragm has to extend 3-5cm. However, the extension vs. load curve flattens out (which is expected [10]) even before 3cm. Hence, the required force would be very high.

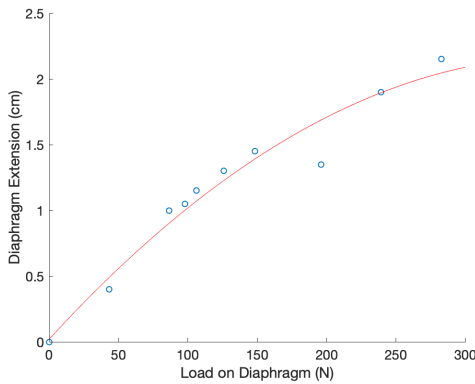


Fig. 6. Extension vs. load curve of rubber diaphragm membrane shows high required force and a levelling-off in the resultant extension.

Additionally, the rubber plastically deformed after a single load cycle (Fig. 7). The edges of the plates also dug into the rubber, leading to concerns over a rupture after repeated loading. Choosing a thinner or lower Shore hardness membrane would lower the force, but would bulge under the weight of the water, and would be even less durable. As the phantom should last thousands of cycles, the low durability, high load requirement, and possibility of sudden catastrophic failure and spill of radioactive water eliminated the rubber diaphragm design.

We therefore designed a piston mechanism instead. This consists of a large cylinder attached directly to the base plate of the phantom. A piston is driven back and forth in the cylinder using a linear actuator to create the volume change. Unlike the



Fig. 7. Diaphragm prototype before (left) and after (right) load testing. Notice the obvious plastic deformation and bulging on the right side.

diaphragm, the piston design has no risk of sudden failure. The actuator force is due to the piston friction and water pressure alone - no rubber has to be stretched - and the only component that can wear out is the O-ring, which is easy to replace.

The mechanism consists of 3 major component types. The piston and cylinder (see Fig. 8), the base and mounting plates, and the linear actuator. Each is described below, before outlining their cumulative capabilities. See Fig. 10 for the assembled mechanism.



Fig. 8. Piston and cylinder with O-rings

1) Piston and Cylinder: A key consideration in the piston and cylinder design was dimensional tolerance and stability. To ensure a good seal, very specific dimensions with low tolerances had to be chosen, according to the Parker O-ring Handbook for dynamic sealing. To achieve and maintain the tight tolerances (eg. ± 0.1 mm over a 14cm diameter) while avoiding scatter artefacts from reflected photons off metal in the reconstructed images, both the piston and cylinder were manufactured from Delrin acetal plastic. Delrin is known to be dimensionally stable and machinable. It has very low water absorption of 0.25% (according to McMaster-Carr), so it will keep its shape when in contact with the water in the phantom. Furthermore, Delrin is very slippery, with friction coefficient of 0.2, which reduces piston-cylinder friction and greatly decreases the required actuator load [9]. Beyond material choice, the cylinder was designed with thick, 27mm walls to avoid any warping. A 3.8mm long chamfer at the mouth of the cylinder ensures easy insertion of the piston without scratching any of the surfaces important for the seal.

Two conflicting factors played a role in determining the inner diameter of the cylinder. The larger the diameter, the smaller the piston displacement has to be for a given volume change, and thus the lower the speed requirement on the linear actuator. However, a larger piston is harder to machine within tolerance and to fit onto the base plate. A diameter

of 14cm was chosen as a compromise. Additionally, at this diameter, the piston displacement for a given volume change corresponds with the axial lung extension for a given tidal volume, as found by O.L. Wade [20]. For example, a piston movement of 33mm leads to a volume change of 500ml, both of which are typical values for relaxed breathing in an adult. Hence, the lungs can be directly coupled to the piston to ensure they have an anatomically accurate flex pattern, as discussed in Section III. This is achieved using ≤ 1 mm thick cables that are not visible on PET scans and do not contribute significantly to gamma photon attenuation. Ultimately, with the chosen dimensions,

$$\Delta V = \frac{\pi}{4} D^2 \Delta x = \frac{\pi}{4} (14\text{cm})^2 (\Delta x) \quad (1)$$

Where ΔV is the torso's (and thus also lungs') volume change and D , Δx are given in Fig. 3. The system's stroke is 8cm, so tidal volumes of up to 1232ml are possible, which constitute realistic deep breaths.

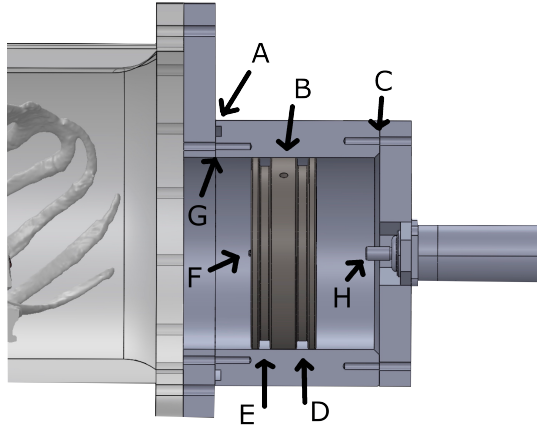


Fig. 9. Cross-section of the piston drive mechanism. A: Cylinder face O-ring groove. B: Inter-O-ring vent hole. C: Actuator mounting plate screw holes. D: Backup O-ring groove. E: Main O-ring groove. F: Insert for mounting piston-lung motion-coupling cable. G: Cylinder to base plate mounting screw holes. H: Linear actuator threaded, male rod end mates directly with piston.

The piston has 2 O-ring grooves which ensure alignment inside the cylinder and provide a watertight dynamic seal (Fig. 9). The actuator-side groove is 6% (0.4mm) deeper, allowing for smaller %-compression in the backup O-ring. This reduces the friction slightly but maintains enough of a seal to be a useful backup. A vent hole connects the inter-O-ring space with the atmosphere in order to avoid pressure traps which can occur in double O-ring configurations. The chosen O-rings are size -429, which have the largest cross-section for the diameter, and thus provide a large contact patch and effective sealing. To compromise between breakaway friction and running friction, 70A durometer Buna-N rubber O-rings were chosen. Buna-N rubber is stronger and more resilient and puncture resistant than other rubbers, making it a good choice for this wear-intensive application. In addition, it is used to make protective gloves in the nuclear industry and will not break down due to radiation, which is important in

the phantom. X- and circular-profile rings were tested, but no major difference in performance was detected.

The cylinder's inner surface was honed to 8-16 μin RA roughness. An O-ring groove was milled into one end of the cylinder (A in Fig. 9), with the mounting screws located radially inside the groove to avoid leaks through the screw holes. Twelve $\frac{1}{4}\text{-}20 \times 1"$ steel socket-cap screws fasten the cylinder to the base plate. The actuator mounting plate is attached in the same manner, but with no O-ring, and the flanged actuator is mounted directly to this plate. In this way, misalignment is minimized, and the whole structure is modular and easy to assemble and disassemble, for example to add or remove O-rings. The linear actuator has an M12 \times 1.75 threaded male rod end, which screws directly into the piston, leaving minimal clearance between piston and mounting plate in order to maximize the positional range of the piston. An identical threaded hole was made on the opposite side of the piston, into which an insert can be screwed to attach a cable to the lungs. Alternatively, a rod can be attached here to move an internal diaphragm, or the hole can be left empty. This gives flexibility in mounting and motion options.

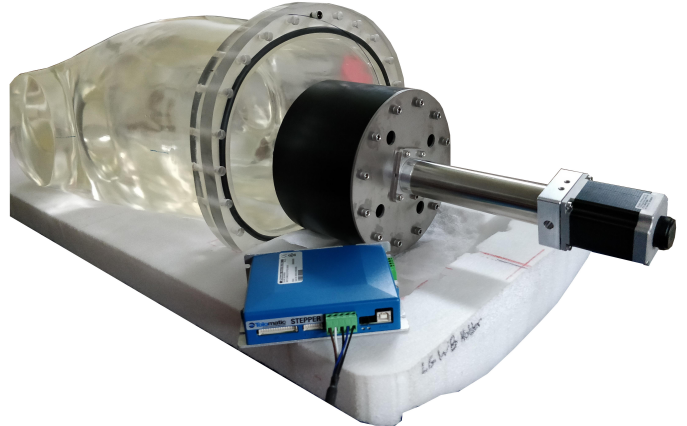


Fig. 10. Assembled breathing mechanism with empty phantom.

2) Mounting Plates: Two plates were made to mount the respiration mechanism to the existing DANN phantom, and to attach the linear actuator to the cylinder assembly. To ensure compatibility with DANN, a CT scan was taken of the phantom, and the base dimensions extracted as a SolidWorks file. The plate was fabricated from 1" thick polycarbonate to withstand the internal pressure and avoid gamma scatter and attenuation artefacts caused by metal. While the overall shape could be made using a waterjet cutter, a mill had to be used for all the screw holes since the waterjet piercing the thick, relatively brittle plastic caused local shattering. A large, central hole was included for the cylinder, as well as $36 \frac{1}{4}\text{-}20$ holes for mounting the cylinder and the phantom base flange in a secure, sealed manner with the load distributed evenly.

As the second plate is relatively far away from the scanner, and supported fully by the cylinder, it was fabricated from 3mm-thick aluminum for weight, strength, and ease of fabrication. The plate was entirely waterjet cut, and included mounting points for the cylinder and actuator. The actuator has a front flange which is mounted directly to the plate to

minimize the risk of misalignment. Furthermore, 4 additional holes were included to provide venting for the piston and avoid pressure build-up. Though no O-ring is present, this plate effectively seals in any small leaks that potentially make it through the piston O-rings, thus preventing contamination of the scanner and environment.

3) Linear Actuator: To move the piston, a lead screw mechanism was chosen because of its superior controllability over pneumatic cylinders and other linear actuators. The actuator was selected based on the criteria outlined in Table II, as well as cost. The derivation of these requirements and details on the actuator performance follow the table.

Criterion	Desired	Chosen Actuator
Speed	54mm/s	167mm/s
Stroke	90mm	90mm
Force	900N	890N
Duty Cycle	100%	100%
Durability	High	5200-scan estimated life
Controllability	High	See below
Weight	Low	$\approx 1.5\text{kg}$

TABLE II
LINEAR ACTUATOR DESIGN REQUIREMENTS

In Section I-B, we set out to achieve a 1000ml tidal volume at 25 breaths per minute. While the piston was designed to provide up to 1232ml tidal volume, and the 90mm actuator stroke supports the full range of piston motion, the actuator must be fast enough to reach 25 breaths per minute at this amplitude. By using Equation IV-1 and noticing that a single breath involves both extension and retraction of the actuator, we find an expression for speed, \dot{x} , in mm/s as a function of breathing rate, ν , and amplitude, V , in breaths per minute and ml:

$$\dot{x} = \frac{2\nu V}{\frac{\pi}{4}14^2 \cdot 60} \approx \frac{\nu V}{461.8} \text{mm/s} \quad (2)$$

Hence, to fulfil the design objective, a linear speed of at least 54mm/s is required.

The required force is the sum of the piston friction (F_f), the water inertia (F_i), and the elastic stretching of the lungs (F_e):

$$F = F_f + F_i + F_e \quad (3)$$

From the Parker O-Ring Handbook, $F_f = f_c L_p + f_H A_p$ where (assuming we are using the -429 O-ring):

Parameter	Value	Meaning	Source
f_c	0.933	O-ring compression friction	Fig. 5-9
L_p	17.29in	Seal rubbing surface length	Tab. 5-4
f_H	10	Fluid pressure friction	Fig. 5-10
A_p	3.97	Projected seal area	Tab. 5-4

TABLE III
PISTON FRICTION PARAMETERS FROM PARKER O-RING HANDBOOK

Thus, the approximate piston friction is $F_f = 250\text{N}$.

To calculate the inertial force, assume the actuator accelerates to the 54mm/s velocity within 0.5cm. This corresponds to an acceleration of $a = \frac{(0.054\text{m/s})^2}{2 \cdot 0.005\text{m}} = 0.292\text{m/s}^2$. While most of the water in the phantom does not move much during the acceleration, at least the water that was in the piston will be accelerated, in addition to some water outside. Suppose, then, that the total volume of water being accelerated is twice the maximum tidal volume - i.e. 2000ml - which is 2kg. Then

$$F_i = (0.292\text{m/s})(2\text{kg}) = 0.58\text{N} \quad (4)$$

This is negligible compared to the frictional force. Even if we took the whole 17.3kg of water to be accelerating, it would still only constitute 5N. This can therefore be ignored. Similarly, the static pressure on the piston can be ignored because the lungs in the water are at atmospheric pressure, and the piston sits at almost the same height as the lungs. Thus, the water pressure on the front of the piston and the air pressure on the back effectively cancel out.

The pressure required to stretch the lungs is more difficult to derive. To simplify the problem, let us assume that the lungs are cylindrical, and use the thin-wall approximation to find the hoop stress in one lung. This, however, also assumes that Hooke's Law holds for rubber-like elastomers. Merrit and Weinhaus [10] found that this is not the case, and that after an initial linear section, the required pressure to increase the radius sharply falls off. Thus, Hooke's Law only provides a conservative estimate. Let ℓ, r, t be the cylindrical lung's length, radius, and wall thickness respectively, and $\ell_0 = 200\text{mm}$, $r_0 = 52\text{mm}$, and $t_0 = 2\text{mm}$ be the initial values. These give the expected initial volume of 1700ml, as well as an initial material volume of $V_0^{mat} \approx 2\pi r_0 t_0 (\ell_0 + r_0) = 21000\text{mm}^3$. Using the incompressibility of rubber, $V_0^{mat} = V_f^{mat}$, so the wall thickness relates to the length and radius by:

$$t \approx \frac{21000}{r(\ell + r)} \quad (5)$$

Now using hoop stress, $\frac{r\Delta P}{t} = \sigma_H$, and Hooke's Law, $\sigma_H = \epsilon_H E = \frac{t_0 - t}{t_0} E$, we obtain an expression for the required pressure differential applied by the piston:

$$\Delta P = \frac{t(t_0 - t)}{rt_0} E \quad (6)$$

Combining Equations 5 and 6:

$$\Delta P = \frac{21000}{r^2(\ell + r)} \left(1 - \frac{21000}{rt_0(\ell + r)} \right) E \quad (7)$$

This pressure is exerted evenly across the surface of the piston, so using $F = PA$ we find F_e :

$$F_e = (0.14)^2 \frac{\pi}{4} \frac{21000}{r^2(\ell + r)} \left(1 - \frac{21000}{rt_0(\ell + r)} \right) E \quad (8)$$

The elastic modulus, E , of silicone rubbers can be estimated roughly from the Shore A durometer using Ruess' Equation: $\log_{10} E = 0.0235S - 0.6403$ [8]. Since the lung silicone has Shore A hardness 35, $E \approx 1.5\text{MPa}$. Thus we can finally calculate the force required to stretch the lungs. We want a

1000ml volume increase and about 6.6cm lung extension [20], so we take $\ell = 266\text{mm}$ and $r = 56.8\text{mm}$. Then $F_e = 199\text{N}$.

According to Equation 3, then, a conservative estimate for the maximum force required from the actuator is $F = 450\text{N}$. Applying a factor of safety of 2, considering that these calculations were approximate, piston friction could increase with wear, foam around the lungs could increase the pressure requirement, and a second O-ring could be added, with unknown effect, the linear actuator should be able to supply around 900N of force.

The desired duty cycle, or ratio of running time to resting time of the actuator, is more easily derived. The phantom has to breathe continuously for the duration of the scan, which can be around 30 minutes, so the duty cycle has to be 100% for extended periods of time. Many actuators use ACME screws, a specific thread geometry which can only operate at about 15% duty cycle. Instead, a ball screw mechanism, which has much less friction, allows for continuous use and a long lifetime.

Based on these criteria, an ERD15 (Tolomatic, USA) ball-screw linear actuator was chosen, along with a Nema-23, 2-stack stepper motor with encoder feedback. This relatively low-cost actuator is designed to run continuously all day and fulfills the load, stroke, and speed requirements. Assuming we carried out 30 minute scans at the calculated force, at 25 breaths per minute and 1000ml tidal volume, the actuator would have an estimated life of 5200 scans (See Fig. 11). The ERD's low profile and simplicity allow it to be mounted as seen in Fig. 10.

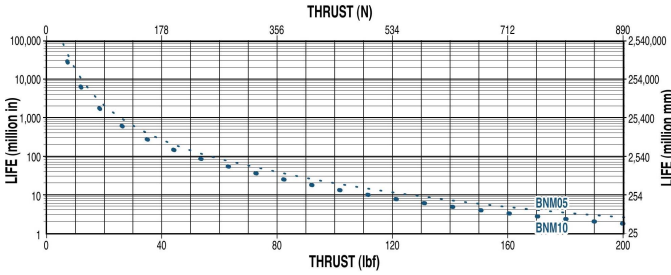


Fig. 11. Tolomatic ERD15 BNM05 actuator expected life. At 450N, the life is 508 million mm, which corresponds to about 5200 scans. (Image from Tolomatic.com)

According to the manufacturer specifications from Tolomatic, the actuator position is accurate to within 0.03mm per cm of movement [31], which translates to a volumetric error of up to 0.3ml per 100ml volume change, using Equation IV-.1. In addition, the 1.8°/step stepper motor combined with the 5mm-lead ball screw mechanism, as well as 2000-count encoder feedback facilitate exact velocity and acceleration control. Hence, the lung motion is precise, consistent, and repeatable.

V. SOFTWARE AND ELECTRICAL DESIGN

The Tolomatic ERD15 actuator is driven by a stepper motor with encoder feedback, which is in turn powered by a 120W, 2.5A, 48V power supply, and controlled by stepper driver hardware from Tolomatic. This hardware provides a few methods for control. First, a free Windows application can be

used to communicate with the driver over USB to configure the actuator. This will be explored in depth below (Section V-A). The second option is analog position control. A 0-10V analog signal can be input to the driver, which moves to the corresponding position (See Section V-B). Control through ethernet and Modbus RTU over RS-485 are also possible, but neither was investigated.

Ultimately, the goal in this control system is to create realistic, consistent, repeatable lung motion with flexibility in breathing rate and amplitude, as well as the ability to include breathing inconsistencies for added realism. Two distinct control methods were created for the phantom and are described below.

A. USB Interface

The actuator manufacturer provides a software interface called Tolomatic Motion Interface (TMI) to communicate with its stepper controllers over USB. While the software is primarily used to configure the driver by setting acceleration, deceleration, maximum velocity, error states and more, it can also be used to directly control the actuator's movement. In 'Indexing Mode', up to 16 moves can be defined, each with a certain acceleration, deceleration, velocity, and goal position. Any of these moves can then be chosen and combined in any order to form a repeating series of up to 16 moves. Taking the simplest example, one may define just 2 moves, one to 45mm, and one to 1mm, and cycle between these two positions indefinitely. By combining more positions, however, and altering their accelerations and decelerations, a very wide variety of breathing patterns can be achieved, including realistic respiratory cycles.

The problem with this method is that visualizing what the respiratory cycle will look like based on a series of linear position, velocity, and acceleration values is difficult. A graphical user interface (GUI) was therefore developed to allow motion planning and visualization, as seen in Fig. 12.

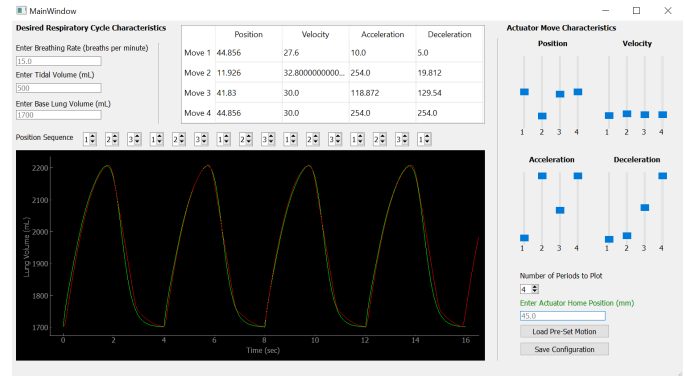


Fig. 12. Screenshot of motion planning application.

In the application, the user can define the breathing rate, amplitude, and base lung volume. Anatomically realistic respiratory curves with these characteristics are automatically generated in green by scaling and shifting the following rational equation (Eq. 9), which was derived from measured breathing curves using MATLAB, and compared to previous models of respiration [18].

$$x = e^{-1.71668t} \frac{0.0106 + 2.3313t + 0.535t^2 + 3.9594t^3}{2.3062 + 0.3517t - 0.6487t^2 + 0.1177t^3} \quad (9)$$

The user can then define up to 4 moves with position, velocity, acceleration, and deceleration, and place them in any order. The corresponding motion profile is generated through iterative kinematic simulation of the actuator, and plotted in real time as the parameters are changed. With the red actuator plot overlaid onto the green desired plot, the optimal set of motion parameters can be determined. It is also possible to save configurations in automatically-formatted JSON files to be re-loaded later.

This control method is simple because the respiratory cycle is visualized, input into user-friendly software, and relayed to the actuator directly over USB. While a variety of motions can be achieved in this manner, it is nonetheless limited by the discrete nature of a set of individual moves. To overcome this problem, at the cost of simplicity, analog control can be used.

B. Analog Position Control

The ERD15 actuator can be controlled using a 0-10V analog signal. The voltage range is mapped onto the positional range of the actuator so that a given voltage causes the actuator to move to that position. The move occurs with predefined acceleration, deceleration, and maximum velocity, which can be configured using the Tolomatic Motion Interface software, but is non-blocking; i.e. a new position command can be given before the current position has been reached, and the actuator will immediately move towards the new position. In this way, arbitrary continuous waveforms can be realized by the actuator, as long as they do not exceed the configured acceleration and velocity values.

Fig. 13 shows the setup used to generate the analog signal. The voltage range is configurable using the Tolomatic software, and was set to 0-3.3V, which was provided by an MCP4725 Digital to Analog Converter (DAC), controlled via the I2C GPIO pins of a Raspberry Pi microcomputer. The encoder feedback is read by the Raspberry Pi, and any control software is run on the Pi.

In order for the actuator to respond to the analog input voltage, analog control must be enabled through a digital input. The digital I/O operates on 28V logic (18-28V is considered high) with respect to the digital common pin (COM). Thus, digital COM is tied to the power supply ground, and a voltage divider is used to provide the 24V needed to enable motion. An N-channel MOSFET whose gate voltage is set by the Raspberry Pi switches the enable input between 0 and 24V. The MOSFET gate is pulled down to ground through a $1\text{M}\Omega$ resistor and attached to the Pi through a 100Ω resistor to prevent parasitic ringing. The voltage divider uses $100\text{k}\Omega$ resistors so the maximum current draw is 0.24mA, which does not affect the operation of the actuator.

With this setup, arbitrary waveforms can be saved as CSV files on the Raspberry Pi. A Python program converts the volumetric data to actuator positional curves using the piston geometry, and then to voltages using the voltage-position

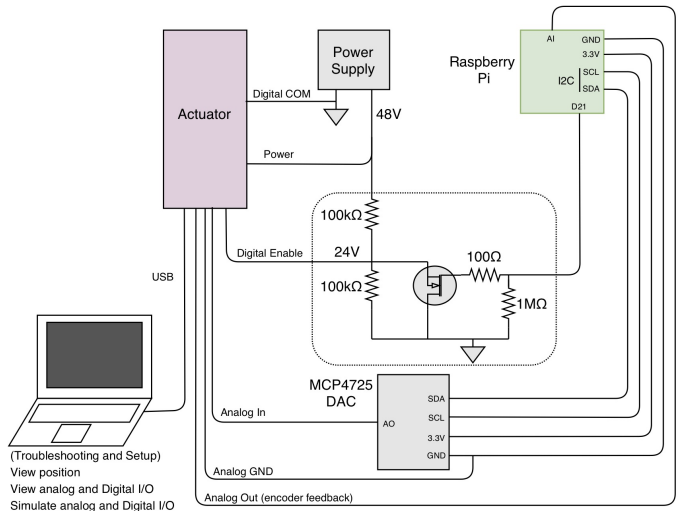


Fig. 13. Schematic of analog position control setup

mapping. The voltages are sent discretely via I2C to the DAC, where they are converted to analog voltages and input into the actuator, thus generating the desired lung motion.

VI. TESTING AND VALIDATION

To validate the efficacy of the piston design, it is essential to perform a number of tests. Given the current Covid-19 situation (at the time of writing, March-April 2020), we have so far been able to complete a subset of these tests, which show that the phantom works as expected. First we set up the phantom in the single O-ring configuration and filled it with water. Filling was straightforward using the neck ports, and no leaks were observed. The piston was then run back and forth continuously for 30 minutes. Again, no leakage was observed.



Fig. 14. Two screen grabs from the breathing test with a balloon. The left side is at maximum inhalation, while the right is maximum exhalation. The volume difference between the two is about 677ml.

Due to the pandemic, the lungs were not available to test the breathing principal, so we used a household balloon. The piston was set to move at 50mm/s, with a 44mm amplitude, which corresponds to an expected volume change of 677ml at over 34 breaths per minute. The balloon was filmed from three directions. Using frame grabs of the video (Fig. 14), the

balloon's inflated and deflated dimensions were ascertained. Assuming the balloon is approximately an ellipsoid, its semi-major axes were [6cm,6cm,8cm] for the inflated lung, and [4.5cm,4.5cm,6cm] for the deflated lung. This corresponds to a 698ml volume change. Given the relatively imprecise measurement method, this is close to the expected volume and confirms that the breathing method was working.

After a total of 40 minutes of almost continuous motion, the phantom was emptied, and the drive mechanism was dismantled and inspected. There were no signs of wear in the mechanism, which would have indicated a problem. The O-ring remained very well lubricated, and the cylinder wall behind the O-ring was dry (Fig. 15). A single smear of water was observed on the rear face of the cylinder, where it had been trapped by the aluminum mounting plate. Overall, this is a positive result, as the phantom lost a single drop of water over 40 minutes of continuous use, and the leaked drop was still contained within the piston mechanism. With continued good lubrication and occasional O-ring replacement, leakage will not increase with use. Since the phantom is left in isolation until the isotopes have decayed to background levels, isolated drops getting through the piston is not a worry as long as they remain contained within the cylinder. However, the second O-ring can also be installed on the piston to further improve the seal.

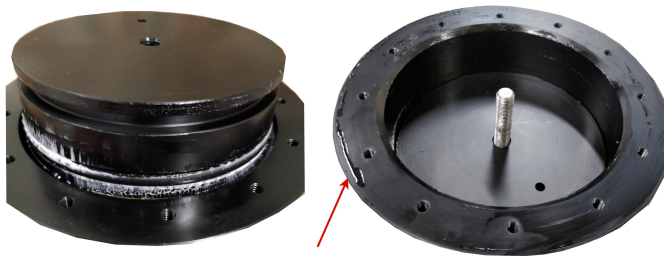


Fig. 15. The dismantled drive mechanism after 40 minutes of continuous use with water. The piston on the left shows a still well lubricated O-ring. The rear surface of the cylinder has a single smear of water on it, indicated by the red arrow. All other liquid-like residue is lubricant.

Having confirmed the efficacy of the piston mechanism and lung motion, the next steps would be to test the actual lungs. While arrangements had been made to fabricate the lungs at Barber Prosthetics (Vancouver, Canada), and we 3D-printed the negative mold, these plans did not go ahead during the pandemic. Once we are able to manufacture the lungs, we will redo the previously described tests but using the actual lungs instead of a balloon. Furthermore, we will test the effect of the foam to see which configuration is more feasible (see Section II). Finally, a CT scan will be taken of the phantom to check anatomy and more precisely characterise the motion, and of course PET scans will be taken to test the design for PET compatibility, material selection, image artefacts, and the effect of the breathing.

VII. CONCLUSION

In this work we presented the mechanical design of an anthropomorphic phantom with realistic anatomy and respiratory motion. The phantom can achieve a variety of respiratory

wave-forms with up to 25 breaths per minute at 1232ml tidal volume. A software interface was developed to plan and visualize these breathing patterns, and two separate control schemes were proposed. Though the breathing concept and mechanism were shown to be effective, some testing and manufacturing remain to be done due to the Covid-19 pandemic. The lungs have to be rolled and connected via custom-designed fittings to breathing tubes and the neck ports of the phantom. Subsequently, lung-piston motion coupling and the use of foam in the torso should be tested, before ultimately verifying the phantom's efficacy in PET and CT scans.

One limitation of the phantom is the lack of cardiac motion. However, there is sufficient space and available ports in the phantom that this could be added. Furthermore, as the lungs are full of air, their 511keV attenuation coefficient is close to 0, whereas in reality, it should be around 40% that of soft tissue [7]. This should be corrected if possible, though previous work has shown this to be difficult [17]. To further develop the phantom, tests with non-uniform lung wall thickness, motion coupling, and the inclusion of foam, as well as improvements to the software interface can all be carried out. Future work with this phantom will of course also include studies on the effects of motion on image quantification.

VIII. OPEN SOURCE

To promote further development of PET and phantom technology, we have open-sourced the entire design, including all CAD files, code, engineering drawings, and more, with supporting documentation. This material can be found here: <https://github.com/dgblack/robotPhantom>.

ACKNOWLEDGMENT

The authors would like to thank Barber Prosthetics, Vancouver, Canada, for their support in silicone rolling and lung manufacture, and for allowing us to use their molding facilities. In addition, Robert de Rot at PQ Systems Ltd., Vancouver, Canada was very helpful in selecting the linear actuator and generously lent us a demo unit during its fabrication. Finally, the guidance and support of the UBC Engineering Physics Project Lab team was invaluable.

REFERENCES

- [1] A. Kesner, C.R. Schmidlein, C. Kunter. 'Real-time data-driven motion correction in PET'. *European Journal of Nuclear Medicine and Molecular Imaging*. 2019, vol. 6, no. 3.
- [2] A. Kesner, J.H. Chung, K.E. Lind, J.J. Kwak, D. Lynch, D. Burckhardt, P.J. Koo, 'Validation of Software Gating: A Practical Technology for Respiratory Motion Correction in PET'. *Radiology*. 2016, vol. 281, no. 1.
- [3] A. Pepin, J. Daouk, P. Bailly, S. Hapdey, M.E. Meyer. 'Management of respiratory motion in PET/computed tomography: the state of the art.' *Nuclear Medicine Communications*. 2014, vol. 35, no. 2, pp. 113-122.
- [4] A. Rahmim, O. Rousset, H. Zaidi. 'Strategies for Motion Tracking and Correction in PET', *PET Clinics*. 2007, vol. 2, no. 2, pp. 251-266.
- [5] C. Huang, Y. Petibon, J. Ouyang, T.G. Reese, M.A. Ahlman, D.A. Bluemke, G. El Fakhri. 'Accelerated acquisition of tagged MRI for cardiac motion correction in simultaneous PET-MR: phantom and patient studies'. *Medical Physics*. 2015, vol. 42, pp. 1087-1097.
- [6] D.J. Kadrmas, M.E. Casey, M. Conti, B.W. Jakoby, C. Lois, D.W. Townsend. "Impact of time-of-flight on PET tumor detection." *Journal of Nuclear Medicine*. 2009, vol 50, pp. 1315-23.

- [7] D.J. Kadrmas, M.E. Casey, N.F. Black, J.J. Hamill, V.Y. Panin, M. Conti. "Experimental comparison of lesion detectability for four fully-3D PET reconstruction schemes." *IEEE Trans Med Imaging*. 2009, vol 28, pp. 523–34.
- [8] K. Larson. "Can you estimate modulus From durometer hardness for silicones?". Dow. 2019. <https://www.dow.com/content/dam/dcc/documents/en-us/tech-art/11/11-3716-01-durometer-hardness-for-silicones.pdf?iframe=true>
- [9] D.V. Bhatt, K.N. Mistry. "Experimental study of friction under different variables on a piston-cylinder assembly." Department of Mechanical Engineering. National Institute of Technology, India.
- [10] D.R. Merrit, F. Weinhaus. "The pressure curve for a rubber balloon." *American Journal of Physics*. January, 1978.
- [11] F. Nayyeri. 'A review on motion correction methods in PET/CT images for detection of cancer cells'. *Acta Medica Bulgarica*. 2015, vol. 42, no. 2.
- [12] I. Chrysanthou-Baustert et al. 'Characterization of attenuation and respiratory motion artifacts and their influence on SPECT MP image evaluation using a dynamic phantom assembly with variable cardiac defects'. *Journal of Nuclear Cardiology*. 2017, vol. 24, pp. 698–707.
- [13] IMV. "PET imaging market summary report." <https://imvinfo.com/product/pet-imaging-market-summary-report-2019>
- [14] I.S. Klyuzhin. "Deformable motion correction and spatial image analysis in positron emission tomography." Thesis, *University of British Columbia*. 2016.
- [15] J.I. Gear, C. Long, D. Rushforth, S.J. Chittenden, C. Cummings, G.D. Flux. "Development of patient-specific molecular imaging phantoms using a 3D printer." *Int. Journal of Medical Physics*. 2014, vol. 41.
- [16] J.J. Visser, E.B. Sokole, H.J. Verberne, J.B. Habraken, H.J. van de Stadt, J.E. Jaspers, M. Shehata, P.M. Heeman, B.L. van Eck-Smit. 'A realistic 3D gated cardiac phantom for quality control of gated myocardial perfusion SPET: the Amsterdam gated (AGATE) cardiac phantom'. *European Journal of Nuclear Medicine and Molecular Imaging*. 2004, vol. 31, pp. 222–228.
- [17] K. Bolwin, B. Czekalla, L.J. Frohwein, F. Büther, K. Schäfers. "Anthropomorphic thorax phantom for cardio-respiratory motion simulation in tomographic imaging." *Physics in Medicine and Biology*. 2018, vol. 63, no 3.
- [18] L.B. Cook. "Rebreathing in the Mapleson A, C and D breathing systems with sinusoidal and exponential flow waveforms". *Anaesthesia*. 1997, vol. 52, pp. 1182–1194.
- [19] L. Guerra, E. De Ponti, F. Elisei, et al. "Respiratory gated PET/CT in a European multicentre retrospective study: added diagnostic value in detection and characterization of lung lesions". *European Journal of Nuclear Medicine and Molecular Imaging*. 2012, vol. 39, no. 9, pp. 1381–1390.
- [20] O.L. Wade. 'Movements of the thoracic cage and diaphragm in respiration'. *Journal of Physiology*. 1954, vol. 124, pp. 193–212.
- [21] O.V. Olesen, C. Svarer, M. Sibomana, S.H. Keller, S. Holm, J.A. Jensen, F. Anderson, L. Höjgaard. "A moveable phantom design for quantitative evaluation of motion correction studies on high resolution PET scanners." *IEEE Transactions on Nuclear Science*. 2010, vol. 57, no. 3, pp. 1116–1124.
- [22] Mayo Clinic. "Positron emission tomography scan." <https://www.mayoclinic.org/tests-procedures/pet-scan/about/pac-20385078>
- [23] M. Söderfjäll, H.M. Herbst, R. Larsson, A. Almqvist. "Influence on friction from piston ring design, cylinder liner roughness and lubricant properties." *Tribology International*. 2017, vol. 116, pp. 272–284.
- [24] National Institute of Standards and Technology. "X-Ray mass attenuation coefficients." <https://physics.nist.gov/PhysRefData/XrayMassCoef/tab4.html>
- [25] R.E. Schmitz, A.M. Alessio, P.E. Kinahan. "The physics of PET/CT scanners." *University of Washington*.
- [26] R. Manber, K. Thielemans, B.F. Hutton, S. Wan, F. Fraioli, A. Barnes, S. Ourselin, S. Arridge, D. Atkinson. "Clinical impact of respiratory motion correction in simultaneous PET/MR, using a joint PET/MR predictive motion model." *Journal of Nuclear Medicine*. Vol. 59, pp. 1467–1493, 2019.
- [27] S. Gholampourkashi, J.E. Cygler, B. Lavigne, E. Heath. "Development of a deformable phantom for experimental verification of 4D Monte Carlo simulations in a deforming anatomy." *Physica Medica*. 2018, vol. 51, pp. 81–90.
- [28] S. Pallotta, S. Calusi, L. Foggi, R. Lisci, L. Masi, L. Marrazzo, C. Talamonti, L. Livi, G. Simontacchi. "ADAM: a breathing lung for SBRT quality assurance." *Physica Medica*. 2018, vol 49, pp. 147–155.
- [29] S.R. Cherry, M. Dahlbom. "PET: physics, instrumentation, and scanners." *Springer*, 2006.
- [30] T. Boltz, W. Pavlicek, R. Paden, M. Renno, A. Jensen, M. Akay. 'An anthropomorphic beating heart phantom for cardiac x-ray CT imaging evaluation'. *Journal of Applied Clinical Medical Physics*, 2010, vol. 11, pp. 191–199.
- [31] Tolomatic. 'ERD Electric Cylinder Features and Options'. <https://www.tolomatic.com/products/product-details/erd-low-cost-electric-cylinders-for-pneumatic-cylinder-replacement/features-options>
- [32] W. Bai, M. Brady. "Motion correction and attenuation correction for respiratory gated PET images." *IEEE Transactions on Medical Imaging*. 2011, vol. 30, no. 2, pp. 351–365.
- [33] W.H. El-Ratal, P.K. Mallick. "Elastic response of flexible polyurethane foams in uniaxial tension." *Journal of Engineering Materials and Technology*. 1996, vol. 118, pp. 157–161.
- [34] Wikipedia. "Lung volumes." https://en.wikipedia.org/wiki/Lung_volumes
- [35] Y. Rakvongthai, G. El Fakhri. "Magnetic resonance-based motion correction for quantitative PET in simultaneous PET-MR imaging." *PET Clinics*. 2017, vol. 12, pp. 321–327.